CHEMISTRY
A EUROPEAN JOURNAL

ChemPubSoc
Europe

DOI: 10.1002/chem.201303086

Comparison of Gas Sorption Properties of Neutral and Anionic Metal–Organic Frameworks Prepared from the Same Building Blocks but in Different Solvent Systems

Myung-Ho Choi, Hye Jeong Park, Dae Ho Hong, and Myunghyun Paik Suh*[a]

Abstract: Two different 3D porous metal–organic frameworks, $[Zn_4O(NTN)_2]\cdot 10\,DMA\cdot 7\,H_2O$ (**SNU-150**) and $[Zn_5(NTN)_4(DEF)_2][NH_2(C_2H_5)_2]_2\cdot 8\,DEF\cdot 6\,H_2O$ (**SNU-151**), are synthesized from the same metal and organic building blocks but in different solvent systems, specifically, in the absence and the presence of a small amount of acid. **SNU-150** is a doubly interpenetrated neutral framework, whereas **SNU-151** is a non-interpenetrated anionic framework containing diethylammonium cations in the pores. Comparisons of the N_2, H_2, CO_2, and CH_4 gas adsorption capacities as well as the CO_2 adsorption selectivity over N_2 and CH_4 in desolvated **SNU-150′** (BET: $1852\,m^2g^{-1}$) and **SNU-151′** (BET: $1563\,m^2g^{-1}$) samples demonstrate that the charged framework is superior to the neutral framework for gas storage and gas separation, despite its smaller surface area and different framework structure.

Keywords: adsorption · carbon dioxide · cationic guests · gas separation · metal–organic frameworks

Introduction

Metal–organic frameworks (MOFs) have attracted great attention because of their potential applications in gas storage[1–6] and separation.[7–14] The gas adsorption capacities of MOFs are enhanced by the increase in surface areas, presence of accessible metal sites,[6,15] and functional groups.[16] The gas separation capabilities of MOFs, in particular for CO_2 separation from flue gas and landfill gas, are affected by the flexibility of the frameworks[7,17] and the ions or molecules contained in the pores of the MOFs,[18–20] because CO_2 molecules can interact with the MOF much more strongly than other gases because of the high quadrupole moment ($14.3\times10^{-40}\,C\,m^2$) and polarizability ($26.3\times10^{-25}\,cm^3$). Recently, it has been reported that anionic MOFs containing metal cations in their pores show higher gas sorption capacities and significantly enhanced CO_2 adsorption selectivities over other gases than common neutral MOFs.[18] However, the synthetic method for obtaining charged MOFs exclusively from neutral MOFs has not yet been well established. Moreover, simple comparison of the gas sorption properties between charged MOFs and neutral MOFs encounters difficulties owing to the large differences in their framework structures and surface areas, because they are constructed from different metal ions and organic building blocks.

Here, we report two porous MOFs, $[Zn_4O(NTN)_2]\cdot 10\,DMA\cdot 7\,H_2O$ (**SNU-150**) and $[Zn_5(NTN)_4(DEF)_2][NH_2(C_2H_5)_2]_2\cdot 8\,DEF\cdot 6\,H_2O$ (**SNU-151**) (H_3NTN = 6,6′,6″-nitrilotri-2-naphthoic acid, DMA = *N*,*N*-dimethylacetamide, DEF = *N*,*N*-diethylformamide), which are synthesized by using the same metal and organic building blocks but different solvent systems, in particular, in the absence and presence of a small amount of acetic acid (Scheme 1). **SNU-150** is a neutral framework, whereas **SNU-151** is an anionic framework containing diethylammonium cations as guests. Desolvated solid **SNU-151′** ($[Zn_5(NTN)_4][NH_2(C_2H_5)_2]_2$), obtained by supercritical CO_2 treatment, exhibits higher adsorption capacities and higher isosteric heats of H_2, CO_2, and CH_4 gas adsorption, as well as higher CO_2 adsorption selectivities over N_2 and CH_4 gases, than **SNU-150′** ($[Zn_4O(NTN)_2]$), because of the stronger interaction of the gas molecules with the anionic framework and the ammonium cations included in the channels.

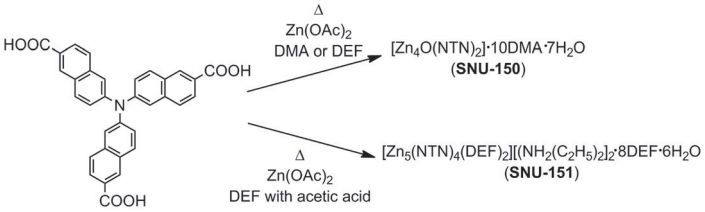

Scheme 1. Preparation of **SNU-150** and **SNU-151**.

Results and Discussion

Synthesis and X-ray crystal structures of neutral (SNU-150) and charged (SNU-151) frameworks: Greenish truncated-oc-

[a] M.-H. Choi, H. J. Park, D. H. Hong, Prof. M. P. Suh
Department of Chemistry, Seoul National University
Seoul 151-747 (Republic of Korea)
Fax: (+82) 2-886-8516
E-mail: mpsuh@snu.ac.kr

Supporting information for this article is available on the WWW under http://dx.doi.org/10.1002/chem.201303086.

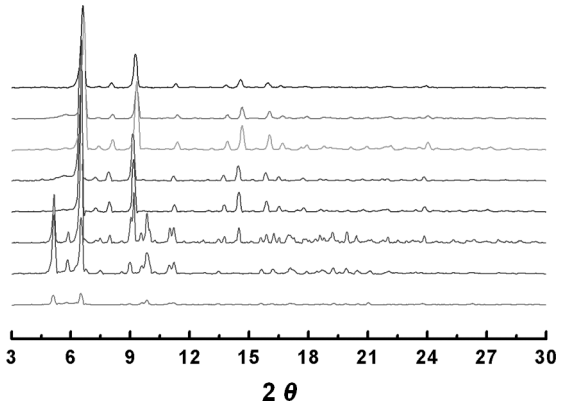

Figure 1. PXRD patterns of the products formed from the solvothermal reaction of $Zn(OAc)_2$ $2H_2O$ (67.3 mg, 0.3 mmol) and H_3NTN (26.3 mg, 0.05 mmol) in DEF (1.5 mL) in the presence of various amount of acetic acid: **SNU-150** is formed in the presence of less than 75 μL (1.3 mmol) of acetic acid, whereas **SNU-151** is formed in the presence of 75 μL (1.3 mmol) to 300 μL (5.2 mmol) of acetic acid. Reaction conditions (from top to bottom): 90 °C, no acid; 90 °C, acetic acid (20 μL); 90 °C, acetic acid (30 μL); 90 °C, acetic acid (50 μL); 90 °C, acetic acid (60 μL); 90 °C, acetic acid (75 μL); 90 °C, acetic acid (250 μL); 90 °C, acetic acid (300 μL).

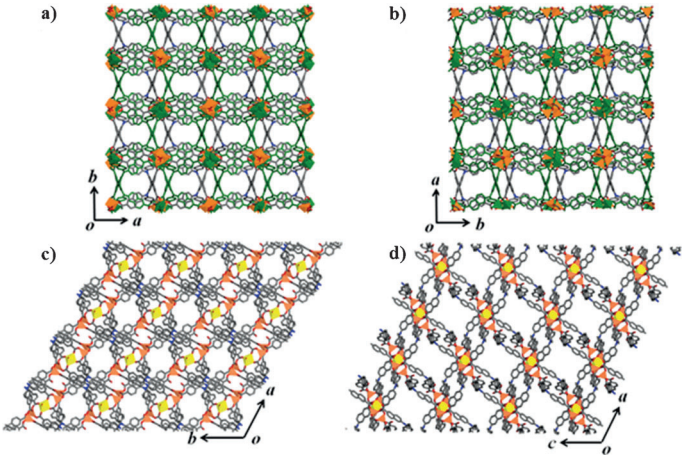

Figure 2. X-ray crystal structures of **SNU-150**, **SNU-150′**, and **SNU-151**. a) View of **SNU-150** on the *ab* plane. b) View of **SNU-150′** on the *ab* plane. c) View of **SNU-151** on the *ab* plane. d) View of **SNU-151** on the *ac* plane. Tetrahedral Zn, orange; octahedral Zn, yellow.

tahedral crystals of **SNU-150** were prepared by heating a DMA solution of $Zn(OAc)_2{\cdot}2H_2O$ and H_3NTN at 90 °C for 24 h. Brown rhombus-shaped crystals of **SNU-151** were synthesized by heating a DEF solution of $Zn(OAc)_2{\cdot}2H_2O$ and H_3NTN in the presence of acetic acid (DEF/acetic acid = 100:3–100:12, v/v) at 90 °C for 24 h. When the volume ratio of acetic acid/DEF was less than 2.4 %, **SNU-150** was formed instead of **SNU-151**, as shown by the powder X-ray diffraction (PXRD) data (Figure 1). That is, the addition of a small amount of acetic acid to the reaction mixture leads to a totally different MOF. **SNU-150** and **SNU-151** are insoluble in common organic solvents.

In the single-crystal X-ray structure of **SNU-150** (Figure 2a), the $Zn_4O(CO_2)_6$ cluster acts as an octahedral secondary building unit (SBU), and NTN^{3-} acts as a triangular organic building block, which results in a (6.3)-connected net with a PdF_2-type net topology, similarly to those reported previously.[21–23] **SNU-150** is doubly interpenetrated, and generates 3D channels that extend along the three orthogonal directions. The effective window size of the channels is 4.5 × 1.7 Å^2. The void volume of **SNU-150** is 49.5 %, as calculated by PLATON (Table 1).[24]

When single crystals of **SNU-150** were activated by using supercritical CO_2 fluid, a desolvated sample of **SNU-150′** was obtained, as shown by IR data, elemental analysis (EA), and thermogravimetric analysis (TGA). Interestingly, **SNU-150** undergoes single-crystal-to-single-crystal transformation during the activation process (Figure 2b). The single-crystal X-ray structure of activated **SNU-150′** exhibits a fine structure that differs from that of **SNU-150**. Many of the key dihedral angles of **SNU-150′** become different from those of **SNU-150**, and the pore size is enlarged to approximately 5.9 × 2.7 Å (compared to 4.5 × 1.7 Å for as-synthesized **SNU-150**) (see Table S1 and Figure S6 in the Support-

Table 1. Crystallographic data of **SNU-150**, **SNU-150′**, and **SNU-151** (squeezed).

	SNU-150	**SNU-150′**	**SNU-151**
formula	$Zn_4C_{66}H_{36}N_2O_{13}$	$Zn_4C_{66}H_{36}$ N_2O_{13}	$Zn_5C_{142}H_{94}N_6O_{26}$
crystal system	cubic	cubic	triclinic
space group	$Ia\bar{3}$	$Pa\bar{3}$	$P\bar{1}$
M_r	1326.45	1326.45	2627.08
a [Å]	27.143(3)	27.3095(6)	16.158(3)
b [Å]	27.143(3)	27.3095(6)	18.171(4)
c [Å]	27.143(3)	27.3095(6)	18.955(4)
a [°]	90	90	99.19(3)
β [°]	90	90	106.28(3)
γ [°]	90	90	116.34(3)
V [Å^3]	19997(4)	20367.7(8)	4518.8(27)
Z	8	8	1
ρ_{calcd} [g cm^{-3}]	0.881	0.865	0.965
T [K]	100(2)	120(2)	100(2)
λ [Å]	0.80003	0.71073	0.69999
μ [mm^{-1}]	1.316	0.970	0.646
GOF (F^2)	1.271	0.999	1.539
F(000)	5360	5360	1346
reflections collected	3912	11598	16832
R_1, wR_2 [$I > 2\sigma(I)$]	0.1107,[a] 0.3329[b]	0.0771,[a] 0.2090[c]	0.1059,[a] 0.3253[b]
R_1, wR_2 (all data)	0.1328,[a] 0.3499[b]	0.0970,[a] 0.2187[c]	0.1120,[a] 0.3371[b]
largest diff. peak/hole [e Å^{-3}]	0.289/−0.350	4.170/−1.125	1.559/−3.119

[a] $R = \Sigma||F_o| - |F_c||/\Sigma|F_o|$. [b] $wR(F^2) = [\Sigma w(F_o^2 - F_c^2)^2/\Sigma w(F_o^2)^2]^{1/2}$ where $w = 1/[\sigma^2(F_o^2) + (0.2000P)^2 + (0.0000)P]$, $P = (F_o^2 + 2F_c^2)/3$ for **SNU-150** and **SNU-151**. [c] $wR(F^2) = [\Sigma w(F_o^2 - F_c^2)^2/\Sigma w(F_o^2)^2]^{1/2}$ where $w = 1/[\sigma^2(F_o^2) + (0.1469P)^2 + (0.0000)P]$, $P = (F_o^2 + 2F_c^2)/3$ for **SNU-150′**.

ing Information), similarly to the case of **SNU-77S**.[21] The powder X-ray diffraction patterns indicate that the framework structure of **SNU-150′** is similar to that of **SNU-150** (Figure 3).

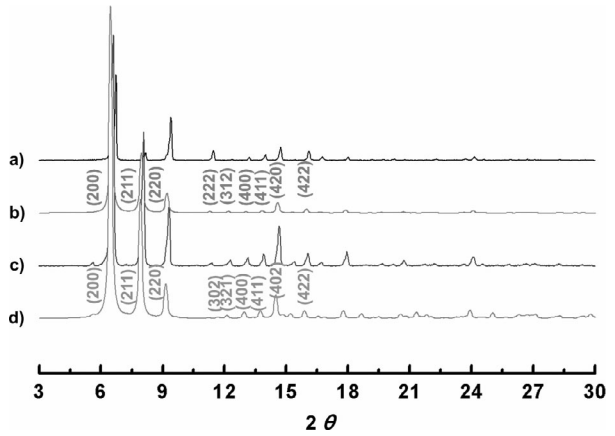

Figure 3. PXRD patterns of a) as-synthesized **SNU-150**, b) simulated powder pattern of **SNU-150** based on its single-crystal X-ray data, c) **SNU-150′** obtained by treatment of **SNU-150** with supercritical CO_2 fluid, and d) simulated powder pattern of **SNU-150′** based on its single-crystal X-ray data.

In the X-ray structure of **SNU-151**, there are three crystallographically independent Zn^{II} centers (Zn1, Zn2, and Zn3), which are linked in the sequence Zn1–Zn2–Zn3–Zn2–Zn1 to form a Zn_5 cluster unit. Zn1 and Zn2 show tetrahedral (td) coordination geometry, being coordinated with four carboxylate oxygen atoms of four different NTN^{3-} ligands. Zn3 shows octahedral coordination geometry, being coordinated with four carboxylate oxygen atoms of four different NTN^{3-} ligands and two oxygen atoms of DEF solvent molecules (see Figure S7 in the Supporting Information). The Zn_5 cluster units are connected by carboxylate groups to form a non-interpenetrated anionic 3D framework generating 2D channels. The effective window sizes of the square channels extending along the *ab* plane and of the cylindrical channels extending along the *ac* plane are 5.2×2.5 and 7.7×6.5 Å^2, respectively (Figure 2c and 2d). Because the Zn_5 metal cluster consists of five Zn^{II} ions and twelve carboxylate groups, two diethylammonium species should be included per formula unit of the host as the counter cationic guests. The chemical formula of **SNU-151** was determined from the EA data as well as the IR spectrum showing ammonium peaks at 2875 cm^{-1}, because the diethylammonium cations could not be refined through single-crystal X-ray diffraction owing to the severe disorder. The void volume of **SNU-151** is 51.5% without taking the diethylammonium guests into consideration. When **SNU-151** was activated by using supercritical CO_2 fluid, two DEF molecules coordinated at the Zn3 atom were removed together with the DEF and water guest solvent molecules included in the channels. The PXRD patterns indicate that the framework structure of **SNU-151′** differs significantly from that of the as-synthesized **SNU-151** (Figure 4).

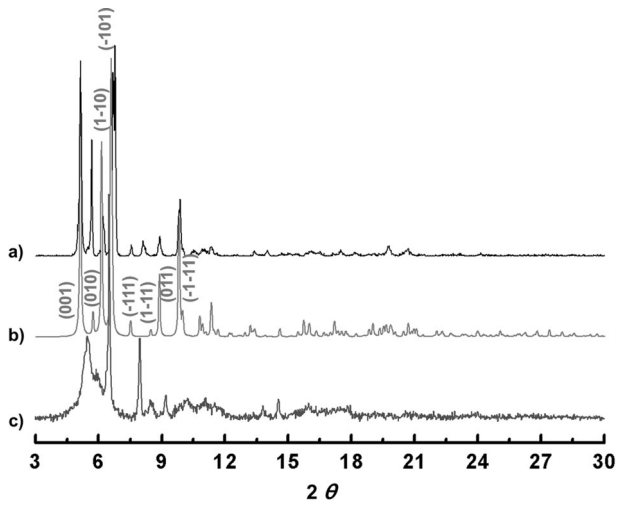

Figure 4. PXRD patterns of a) as-synthesized **SNU-151**, b) simulated powder pattern of **SNU-151** based on its single-crystal data, c) **SNU-151′** obtained from the treatment of **SNU-151** with supercritical CO_2 fluid.

Gas sorption properties: The gas adsorption isotherms of **SNU-150′** and **SNU-151′** were measured for N_2, H_2, CO_2, and CH_4 gases, and the data are summarized and compared with those of the previously reported **SNU-77S**[21] and **SNU-100′**,[18] which have similar structures to **SNU-150′** and **SNU-151′**, respectively (Table 2).

The N_2 sorption isotherms of **SNU-150′** and **SNU-151′** show type-I curves, which are characteristic of microporous materials (Figure 5a). **SNU-150′** shows a small hysteresis of type H-4 in the N_2 desorption curve, which may be associated with the narrow slit-like pores.[25] The BET (Langmuir) surface areas of **SNU-150′** and **SNU-151′** are 1852 (1945) and 1563 (1674) m^2 g^{-1}, respectively. The pore volumes esti-

Table 2. Gas adsorption data of **SNU-150′** and **SNU-151′** together with the comparison with **SNU-77S** and **SNU-100′**.

	T	*P*	Adsorption capacity [wt%]			
	[K]	[atm]	**SNU-150′**	**SNU-77S**[21]	**SNU-151′**	**SNU-100′**[18]
N_2	77	0.95	71.1	131	55.3	26.2
	298	1	0.546	0.40	0.519	0.624
H_2	77	1	1.54	1.79	2.00	1.81
	87	1	1.00	1.01	1.24	1.30
Q_{st} of H_2 adsorption [kJ mol^{-1}]			5.04–4.65	7.05	6.27–5.82	8.14–7.08
CO_2	195	1	78.6	169	67.8	45.2
	231	1	40.5	130	56.0	37.2
	273	1	12.0	8.21	22.2	19.9
	298	1	6.09	3.94	14.1	14.1
Q_{st} of CO_2 adsorption [kJ mol^{-1}]			17.1–16.5	19.9–19.4	27.1–21.0	29.3–27.7
CH_4	195	1	11.1	8.70	11.3	10.4
	231	1	3.15	4.12	7.30	7.57
	273	1	1.29	1.20	2.00	2.56
	298	1	0.859	0.62	1.24	1.41
Q_{st} of CH_4 adsorption [kJ mol^{-1}]			12.8–12.3	14.3–14.2	18.2–16.6	26.5–22.4

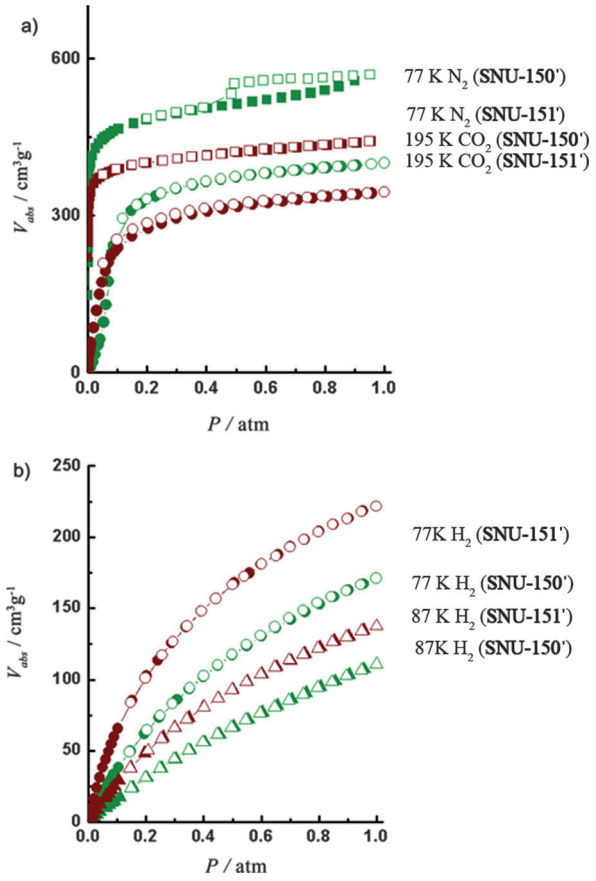

Figure 5. Gas sorption isotherms for **SNU-150′** (green) and **SNU-151′** (burgundy). a) N_2 at 77 K (squares) and CO_2 at 195 K (circles). b) H_2 at 77 K (circles) and 87 K (triangles). Filled shapes, adsorption; open shapes, desorption.

mated by applying the Dubinin–Radushkevich (DR) equation are 0.717 $cm^3 g^{-1}$ for **SNU-150′** and 0.614 $cm^3 g^{-1}$ for **SNU-151′**. The pore-size distributions obtained through the Horvath–Kawazoe (HK) method suggest that **SNU-150′** and **SNU-151′** have pore sizes of 6.18 and 6.08 Å, respectively (Figure 6).[26]

The H_2 adsorption capacities of **SNU-150′** and **SNU-151′** are 1.54 and 2.00 wt %, respectively, at 77 K and 1 atm (Figure 5b). The isosteric heats (Q_{st}) of the H_2 adsorption estimated from the isotherms measured at 77 and 87 K by using a virial equation[27] are 5.04–4.65 kJ mol^{-1} for **SNU-150′** and 6.27–5.82 kJ mol^{-1} for **SNU-151′**, depending on the degree of H_2 loading.

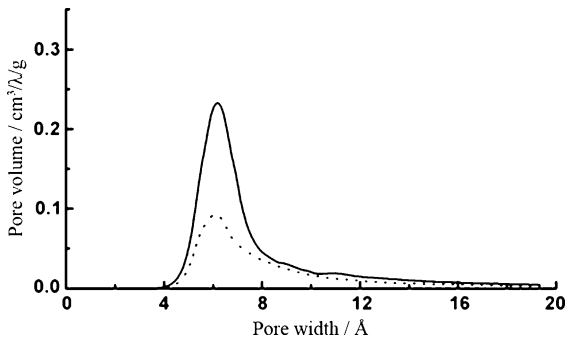

Figure 6. Pore-size distributions of **SNU-150′** (solid line) and **SNU-151′** (dotted line), estimated by using the Horvath–Kawazoe (HK) method using the N_2 sorption data measured at 77 K.

The CO_2 and CH_4 gas adsorption capacities of **SNU-151′** at 1 atm at $T = 231$ and 273 K are higher than those of **SNU-150′**, as shown in Table 2 and Figure 7. At 298 K and 1 atm, **SNU-151′** adsorbs 14.1 wt % of CO_2, which is approximately 2.3 times higher than the CO_2 uptake capacity (6.09 wt %) of **SNU-150′**. The Q_{st} values of the CO_2 and CH_4 adsorptions were calculated by using the Clausius–Clapeyron equation, applying the polynomial equation and Langmuir–Freundlich equation, respectively, to the adsorption isotherms measured at 195, 231, 273, and 298 K. The Q_{st} values of the CO_2 and CH_4 adsorptions in **SNU-151′** are 27.1–21.0 kJ mol^{-1} and 18.2–16.6 kJ mol^{-1}, respectively, which are also higher than those (17.1–16.5 and 12.8–12.3 kJ mol^{-1}, respectively) in **SNU-150′** (see Figure S11 in the Supporting Information).

The higher uptake capacities and higher Q_{st} values for the H_2, CO_2, and CH_4 adsorptions in **SNU-151′** than in **SNU-150′** must be attributed to the stronger interactions of those gas molecules with the anionic framework and diethylammonium cationic guests included in **SNU-151′**, compared to their interactions with the neutral framework of **SNU-150′**.

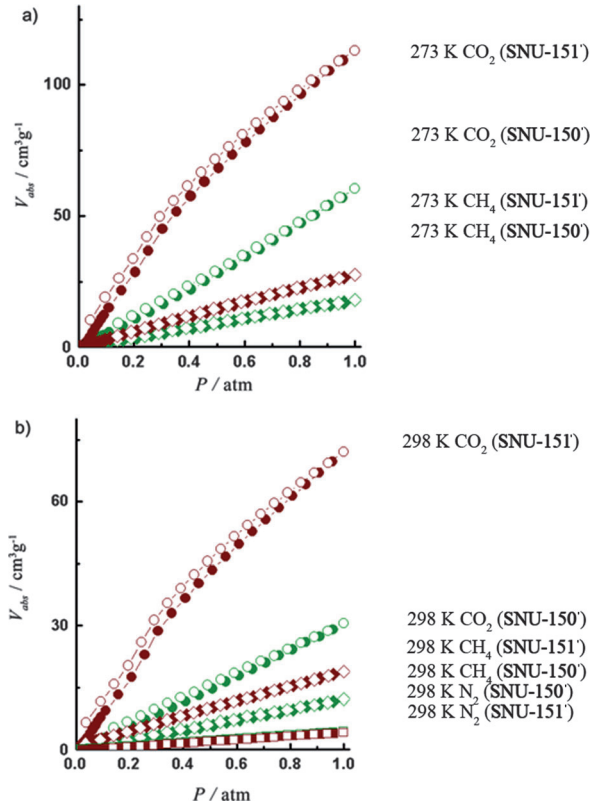

Figure 7. Gas sorption isotherms for **SNU-150′** (green) and **SNU-151′** (burgundy). a) CO_2 (circles) and CH_4 (diamonds) at 273 K. b) CO_2 (circles), CH_4 (diamonds), and N_2 (squares) at 298 K. Filled shapes, adsorption; open shapes, desorption.

In addition, the pore size (6.08 Å) of **SNU-151′** is slightly smaller than that (6.18 Å) of **SNU-150′** as estimated from the N_2 adsorption data (Figure 6), which is also responsible for the higher Q_{st} values of the gas adsorption in **SNU-151′**, even though its activated framework structure is different from that of **SNU-150′**. It is quite well recognized that charged frameworks show superior gas sorption properties to neutral ones.[18,28–30]

When the gas adsorption properties of **SNU-150′** are compared with those of **SNU-77S**,[21] which also has PdF_2 topology, it is found that **SNU-150′** adsorbs much smaller amounts of N_2 and H_2 gases at 77 K and 1 atm, as well as a smaller amount of CO_2 gas at 195 K and 1 atm. This must be attributed to the significantly smaller surface area (1852 $m^2 g^{-1}$) of **SNU-150′** than that (3670 $m^2 g^{-1}$) of **SNU-77S**. When the gas adsorption properties of **SNU-151′** are compared with those of **SNU-100′**, which has an anionic framework with diethylammonium cations, it is observed that **SNU-151′** is superior to **SNU-100′**.[18] This is also attributed to the higher surface area (1563 $m^2 g^{-1}$) of **SNU-151′** than that (814 $m^2 g^{-1}$) of **SNU-100′**. However, at 298 K and 1 atm, the CO_2 and CH_4 gas uptake capacities of **SNU-150′** and **SNU-151′** become comparable to those of **SNU-77S** and **SNU-100′**, respectively.

SNU-150′ and **SNU-151′** adsorb CO_2 gas selectively at 298 K, with hardly any adsorption of N_2 and CH_4 gases (Figure 7b) (see Figure S10 in the Supporting Information). According to the calculation using the ideal adsorbed solution theory (IAST) with the assumption that the flue gas has a CO_2/N_2 volume ratio of 15:85, the selectivity values of the CO_2/N_2 adsorption at 298 K are 30.0 for **SNU-151′** and 5.44–6.42 for **SNU-150′** depending on the pressure (up to 1 atm) (Figure 8). The present result is consistent with our previous report that an anionic framework (**SNU-100′**) with cationic guests showed very high CO_2 uptake selectivity over N_2.[18] The CO_2/N_2 adsorption selectivity of **SNU-151′** is higher than those of **SNU-100′** (26.5)[18] and $H_3[(Cu_4Cl)_3(BTTri)_8]$ (21.0).[31] The selectivity values of the CO_2 adsorption over

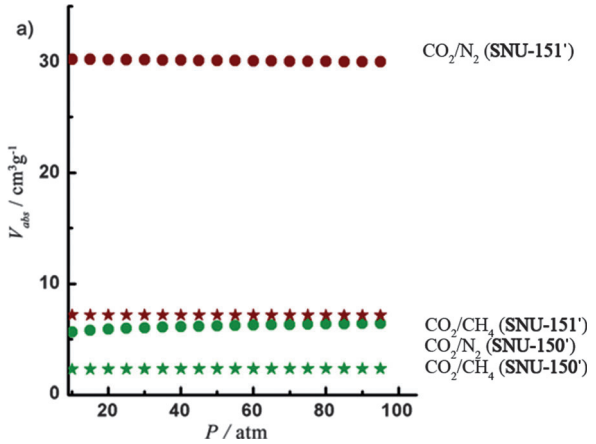

Figure 8. Selectivities of **SNU-150′** (green) and **SNU-151′** (burgundy) for CO_2/N_2 (circles) and CO_2/CH_4 (stars) adsorption depending on the pressure, calculated by using ideal adsorbed solution theory (IAST) with the assumption that the flue gas has a CO_2/N_2 volume ratio of 15:85 and landfill gas has a CO_2/CH_4 volume ratio of 50:50.

CH_4 were also calculated by using IAST with the assumption that the landfill gas has a CO_2/CH_4 volume ratio of 50:50 at 298 K. The values are 7.20 for **SNU-151′** and 2.26–2.35 for **SNU-150′** depending on the pressure (up to 1 atm) at 298 K. **SNU-151′** shows a higher selectivity for CO_2 adsorption over CH_4 than $[Cu(bpy\text{-}2)_2(SiF_6)]$[32] (bpy-2 = 1,2-bis(4-pyridyl)ethene) and the $[Zn_2(BDC)_2(DABCO)]$ (DMOF) series.[33]

Conclusion

We have prepared two different porous MOFs, **SNU-150** and **SNU-151**, from the same metal and organic building blocks but in the presence and absence of acetic acid. **SNU-150** is a neutral framework, whereas **SNU-151** is an anionic framework containing diethylammonium guests. **SNU-150** undergoes a single-crystal-to-single-crystal transformation upon guest removal, which affords **SNU-150′** with a slightly altered structure. **SNU-151′**, which is formed upon the removal of guest solvent as well as coordinated solvent molecules from **SNU-151**, has a different structure from **SNU-151.** **SNU-151′** shows higher uptake capacities for H_2, CO_2, and CH_4 gases as well as higher isosteric heats of those gas adsorptions than **SNU-150′**, despite the smaller surface area of **SNU-151′** (BET: 1563 $m^2 g^{-1}$) than that of **SNU-150′** (BET: 1852 $m^2 g^{-1}$). These properties are attributed to the charged framework and smaller pore size of **SNU-151′**. Furthermore, **SNU-151′** shows a significantly higher CO_2/N_2 adsorption selectivity at 298 K than **SNU-150′**. The present results suggest that for gas storage and gas separation applications, the synthesis of charged frameworks rather than neutral ones should be recommended, regardless of the framework structures.

Experimental Section

General methods: Anhydrous 1,4-dioxane was purchased from Sigma Aldrich, and used without further purification. Other chemicals and solvents used in the syntheses were of reagent grade and were used without further purification. Infrared spectra were recorded with a Perkin–Elmer 2000 FTIR spectrophotometer. Elemental analyses were recorded with a Perkin–Elmer 2400 Series II CHNS/O Analyzer. ^{1}H NMR spectra were measured on Bruker Advance DPX-300 spectrometer (300 MHz) at room temperature. Thermogravimetric analysis (TGA) and differential scanning calorimetry (DSC) were performed under N_2 (g) at a scan rate of 5 °C with a TGA Q50 and DSC Q10, respectively (TA instruments). Powder X-ray diffraction (PXRD) data were recorded on a Bruker D5005 diffractometer at 40 kV and 40 mA (CuK_α, $\lambda = 1.54050$ Å) with a scan speed of 0.5 ° min^{-1} and a step size of 0.02° (2θ).

Synthesis of H_3NTN: H_3NTN (6,6′,6″-nitrilotri-2-naphthoic acid) was prepared as follows through modification of the previously reported methods.[34]

Synthesis of trimethyl 6,6′,6″-nitrilotri-2-naphthoate: Under a N_2 atmosphere, $Pd(OAc)_2$ (129 mg, 0.575 mmol) and *rac*-2,2′-bis(diphenylphosphino)-1,1′-binaphthyl (*rac*-BINAP) (716 mg, 1.15 mmol) were dissolved in anhydrous 1,4-dioxane (100 mL). After stirring for 15 min, methyl 6-bromo-2-naphthoate (8.16 g, 30.8 mmol, 2.8 equiv), methyl 6-amino-2-naphthoate (2.32 g, 11.5 mmol, 1 equiv), and Cs_2CO_3 (5.63 g, 29.2 mmol, 2.5 equiv) were added. The solution was heated at reflux for five days,

cooled to room temperature, and diluted with CH_2Cl_2 (200 mL). The crude mixture was filtered through celite, concentrated through evaporation of the solvent, and then purified by silica gel column chromatography with *n*-hexane/CH_2Cl_2 (2:1, v/v) and then CH_2Cl_2 as eluents. The product was obtained as a light yellow powder. ^{1}H NMR ($CDCl_3$): $\delta =$ 3.99 (s, 9H), 7.44 (d, $J = 8.8$ Hz, 3H), 7.60–7.62 (m, 6H), 7.90 (d, $J =$ 8.9 Hz, 3H), 8.03 (d, $J = 8.6$ Hz, 3H), 8.60 ppm (s, 3H).

Synthesis of 6,6′,6″-nitrilotri-2-naphthoic acid (H_3NTN): Trimethyl 6,6′,6″-nitrilotri-2-naphthalate was dissolved in MeOH, and then a saturated aqueous solution of NaOH was added until the solution reached pH 8. The solution was heated at reflux for one day, and then the solvent was removed by evaporation. The crude product was dissolved with distilled water, and HCl was added until the solution reached pH 2. The solution was cooled to room temperature, and the solid formed was filtered off, washed with water, and dried in vacuo. ^{1}H NMR ([D_6]DMSO): $\delta =$ 7.40 (d, $J = 8.4$ Hz, 3H), 7.64 (s, $J = 35.7$ Hz, 3H), 7.76 −7.90 (m, 6H), 8.00 (d, $J = 9$ Hz, 3H), 8.03 (d, $J = 9$ Hz, 3H), 8.46 ppm (s, $J = 25.8$ Hz, 3H); elemental analysis calcd (%) for $C_{33}H_{21}NO_6$: C 75.13, H 4.01, N 2.66; found: C 73.01, H 4.06, N 2.56.

Synthesis of $[Zn_4O(NTN)_2]\cdot 10DMA\cdot 7H_2O$ (SNU-150): The DMA solution (1.5 mL) of $Zn(OAc)_2\cdot 2H_2O$ (67.3 mg, 0.3 mmol) and the DMA solution (1 mL) of H_3NTN (26.3 mg, 0.05 mmol) were added in a serum glass bottle. The bottle was sealed and heated in an oven at 90 °C for 24 h, and truncated octahedral green crystals of $[Zn_4O(NTN)_2]\cdot 10DMA\cdot 7H_2O$ were obtained. When DEF was used as the solvent instead of DMA with the same reaction mixture, the product was formed as a polycrystalline powder, the PXRD data of which indicated that it had the same framework structure as **SNU-150**. Yield: 42.5 mg (73.2 % based on H_3NTN); FTIR for **SNU-150** (KBr): $\tilde{\nu} =$ 3401 (O−H), 3053 (C−$H_{(NTN)}$), 2931 (C−$H_{(DMA)}$), 1626, 1587 cm^{-1} (O=C−O); elemental analysis calcd (%) for $Zn_4C_{106}H_{140}N_{12}O_{30}$: C 54.78, H 6.07, N 7.23; found: C 54.46, H 5.90, N 7.33.

Preparation of $[Zn_4O(NTN)_2]$ (SNU-150′): Before being dried, crystals of as-synthesized **SNU-150** were transferred into a vial (20 mL) together with the mother liquor. The mother liquor was decanted and the crystals were washed briefly with pure DMA (2×15 mL). The sample was desolvated by using supercritical CO_2 fluid. FTIR for **SNU-150′** (KBr): $\tilde{\nu} =$ 3052 (C−$H_{(NTN)}$), 1623, 1589 cm^{-1} (O=C−O); elemental analysis calcd (%) for $Zn_4C_{66}H_{36}O_{13}N_2$: C 57.67, H 2.64, N 2.04; found: C 57.36, H 2.66, N 2.24.

Synthesis of $[Zn_5(NTN)_4(DEF)_2][NH_2(C_2H_5)_2]_2\cdot 8DEF\cdot 6H_2O$ (SNU-151): The DEF solution (1.5 mL) of $Zn(OAc)_2\cdot 2H_2O$ (67.3 mg, 0.3 mmol) was mixed with the DEF solution (1 mL) of H_3NTN (26.3 mg, 0.05 mmol) in a serum glass bottle, and then acetic acid (0.1 mL) was added. The reaction bottle was sealed and heated in an oven at 90 °C for 24 h, and rhombus-shaped brown crystals of $[Zn_5(NTN)_4(DEF)_2][NH_2(C_2H_5)_2]_2\cdot 8DEF\cdot 6H_2O$ were formed. Yield: 0.0306 mg (67.1 % based on H_3NTN); FTIR for **SNU-151** (KBr pellet): $\tilde{\nu} =$ 3429 (O−H), 3054 (C−$H_{(NTN)}$), 2975, 2935 (C−$H_{(NTN)}$), 2875 (N−$H_{(diethylammonium)}$), 1659 (C=$O_{(DEF)}$), 1625, 1594 cm^{-1} (O=C−O); elemental analysis calcd (%) for $Zn_5C_{190}H_{208}N_{16}O_{35}$: C 61.80, H 5.95, N 6.07; found: C 61.39, H 5.77, N 5.95.

Preparation of $[Zn_5(NTN)_4][NH_2(C_2H_5)_2]_2$ (SNU-151′): Prior to activation, crystals of as-synthesized $[Zn_5(NTN)_4(DEF)_2][NH_2(C_2H_5)_2]_2\cdot 8DEF\cdot 6H_2O$ were transferred to a vial (20 mL) together with the mother liquor. The mother liquor was decanted and the crystals were washed briefly with pure DEF (2×15 mL). The sample was desolvated by using supercritical CO_2 fluid. FTIR for **SNU-151′** (KBr pellet): $\tilde{\nu} =$ 3050 (C−$H_{(NTN)}$), 2853 (N−$H_{(diethylammonium)}$), 1690 (C=$O_{(NTN)}$), 1624, 1590 cm^{-1} (O=C−O); elemental analysis calcd (%) for $Zn_5C_{140}H_{96}O_{24}N_6$: C 65.34, H 3.76, N 3.27; found: C 65.81, H 3.80, N 3.39.

X-ray crystallography: Crystals of $[Zn_4O(NTN)_2]\cdot 10DMA\cdot 2H_2O$ (**SNU-150**) and $[Zn_5(NTN)_4(DEF)_2][NH_2(C_2H_5)_2]_2\cdot 8DEF\cdot 6H_2O$ (**SNU-151**) were coated with Paratone-N oil, and the diffraction data were measured at 100 K with synchrotron radiation ($\lambda = 0.80003$ Å for **SNU-150** and $\lambda =$ 0.69999 Å for **SNU-151**) on an ADSC Quantum-210 detector at 2D SMC with a silicon (111) double crystal monochromator (DCM) at the Pohang Accelerator Laboratory, Korea. The ADSC Q210 ADX program[35] was used for data collection (**SNU-150**: detector distance, 62 mm; omega scan, $\Delta\omega = 1°$; exposure time, 10 s/frame; **SNU-151**: detector distance, 70 mm; omega scan, $\Delta\omega = 1°$; exposure time, 10 s/frame), and HKL3000 sm (Ver. 703r)[36] was used for cell refinement, reduction, and absorption corrections. The diffraction data of the activated sample $[Zn_4O(NTN)_2]$ (**SNU-150′**) were collected at 100 K with an Enraf–Nonius Kappa CCD diffractometer (MoK_a, $\lambda = 0.71073$ Å, graphite monochromator) by coating the crystal with Paratone-N oil. Preliminary orientation matrices and unit-cell parameters were obtained from the peaks of the first ten frames, and then refined by using the whole data set. Frames were integrated and corrected for Lorentz and polarization effects by using DENZO.[36] The scaling and global refinement of crystal parameters were performed by using SCALEPACK.[36] No adsorption correction was made. The crystal structures of **SNU-150**, **SNU-151**, and **SNU-150′** were solved by direct methods[37] and refined through full-matrix least-squares refinement using the SHELXL-97 program.[38] The hydrogen atoms were positioned geometrically by using a riding model. The electron densities of the disordered guest molecules were flattened by using the SQUEEZE option of PLATON.[39] In **SNU-150**, the overall framework was statistically disordered over two sites with 1:1 occupancies. Consequently, all the atoms were given by 0.5 occupancy, except Zn(1), O(1), O(1)′, N(1), and N(1)′, which sit on threefold crystallographic axes, and were given by the occupancy of 1/6. In **SNU-150′**, the site occupancy factors were given as 0.33333 for the Zn(1), O(1), N(1), and N(2) atoms, which sit on threefold crystallographic axes. CCDC-917750 (**SNU-150**), 917751 (**SNU-150′**), and 917752 (**SNU-151**) contain the supplementary crystallographic data for this paper. These data can be obtained free of charge from The Cambridge Crystallographic Data Centre via www.ccdc.cam.ac.uk/data_request/cif.

Supercritical CO_2 activation method: Before being dried, as-synthesized crystals, which were still in the mother liquor, were transferred to a vial (20 mL). The mother liquor was decanted and the crystals were washed briefly with pure solvent (2×15 mL). The crystals were placed inside the supercritical dryer together with the solvent, and the drying chamber was sealed. The temperature and pressure of the chamber were raised to 45 °C and 200 bar with CO_2, above the critical point (31.8 °C, 73 atm) of CO_2. The chamber was vented at a rate of 10 mL min^{-1} and then filled with CO_2 again. The cycles of refilling with CO_2, pressurizing, and venting were repeated for 6 h. After drying, the closed container with the dried crystals was transferred to a glove bag to avoid exposure of the crystals to air. The gas sorption isotherms of the samples were measured without further activation.

Gas sorption measurements: The gas adsorption/desorption experiments were performed with an automated micropore gas analyzer, Autosorb-3B (Quantachrome Instruments). All the gases used were of 99.999 % purity. **SNU-150′** and **SNU-151′** were pre-desolvated by using supercritical CO_2 fluid at 45 °C for 8 h. The predried solid was introduced to a gas sorption cell, the weight of which was measured exactly, and then the gas sorption isotherms were measured. The sample weight was measured precisely after the measurement of gas sorption. Between the experiments with various gases, the out-gassing procedure was repeated for approximately 1 h. The N_2 gas sorption isotherms were monitored at 77 K by using liquid nitrogen, and the H_2 gas sorption isotherms were monitored at 77 and 87 K, at each equilibrium pressure, by the static volumetric method. The adsorption isotherms for CO_2 and CH_4 gases were measured at 195, 231, 273, and 298 K. The sorption properties, including pore volume, pore size, and surface area were analyzed by using Autosorb 1 for Windows 1.24 software.

Estimation of isosteric heats of H_2 adsorption: The isosteric heats (Q_{st}) of H_2 adsorption in **SNU-150′** and **SNU-151′** were estimated from the H_2 sorption data measured at 77 and 87 K. A virial-type expression was used [Eq. (1)], which is composed of parameters a_i and b_i, which are independent of temperature. In Equation (1), P is the pressure (atm), N is the amount of adsorbed H_2 gas (mg g^{-1}), T is the temperature (K), a_i and b_i are the virial coefficients, and m and n represent the number of coefficients required to describe the isotherms adequately. An equation was fit using the R statistical software package.[40]

$$\ln P = \ln N + \frac{1}{T}\sum_{i=0}^{m} a_i N^i + \sum_{i=0}^{n} b_i N^i \quad (1)$$

The values of the virial coefficients, a_0 through a_m, were used to calculate the isosteric heat of adsorption by using Equation (2), in which Q_{st} is the coverage-dependent isosteric heat of adsorption and R is the universal gas constant.

$$Q_{st} = +R\sum_{i=0}^{m} a_i N^i \quad (2)$$

Estimation of isosteric heats of CO_2 and CH_4 adsorptions: The CO_2 adsorption data of **SNU-150′** and **SNU-151′** at 195, 231, 273, and 298 K were fit to a polynomial equation by using the *Origin 8* program, and the CH_4 adsorption data of **SNU-150′** and **SNU-151′** at 195, 231, 273, and 298 K were fit to the Langmuir–Freundlich equation, in which N is the amount of absorbed gas, N_{sat} is the amount of adsorbed gas at saturation, P is the pressure, and b and t are constants [Eq. (3)]. The heat of the gas adsorption was calculated by using the Clausius–Clapeyron equation [Eq. (4)] at each gas loading point.

$$\frac{N}{N_{sat}} = \frac{bP^t}{1+bP^t} \quad (3)$$

$$\frac{\partial(\ln P)}{\partial(1/T)} = -\frac{Q_{st}}{R} \quad (4)$$

Calculation of selectivity of CO_2 adsorption: The selectivities of CO_2 adsorption over N_2 and CH_4 were calculated by using the ideal adsorbed solution theory (IAST),[41] which enables the prediction of adsorption equilibriums of binary gas mixtures from the related single-component isotherms. The CO_2, N_2, and CH_4 adsorption isotherms of **SNU-150′** and **SNU-151′** measured at 298 K were fit to the Allometric1 equation ($y = ax^b$) and polynomial equation, respectively, on a logarithmic scale, and the IAST parameters used in the selectivity calculations were obtained (see Figures S8, S17, and S18 and Tables S2 and S3 in the Supporting Information).

Acknowledgements

This work was supported by a National Research Foundation of Korea (NRF) grant funded by the Korean Government (MSIP) (no. 2012–055324 and no. 2005–0049412). The authors acknowledge the Pohang Accelerator Laboratory (PAL) for the use of the synchrotron beamline.

[1] H. Furukawa, N. Ko, Y. B. Go, N. Aratani, S. B. Choi, E. Choi, A. O. Yazaydin, R. Q. Snurr, M. O'Keeffe, J. Kim, O. M. Yaghi, *Science* **2010**, *329*, 424–428.
[2] M. P. Suh, H. J. Park, T. K. Prasad, D.-W. Lim, *Chem. Rev.* **2012**, *112*, 782–835.
[3] J.-R. Li, R. J. Kuppler, H.-C. Zhou, *Chem. Soc. Rev.* **2009**, *38*, 1477–1504.
[4] K. Sumida, D. L. Rogow, J. A. Mason, T. M. McDonald, E. D. Bloch, Z. R. Herm, T.-H. Bae, J. R. Long, *Chem. Rev.* **2012**, *112*, 724–781.
[5] Y. E. Cheon, M. P. Suh, *Angew. Chem.* **2009**, *121*, 2943–2947; *Angew. Chem. Int. Ed.* **2009**, *48*, 2899–2903.
[6] Y.-G. Lee, H. R. Moon, Y. E. Cheon, M. P. Suh, *Angew. Chem.* **2008**, *120*, 7855–7859; *Angew. Chem. Int. Ed.* **2008**, *47*, 7741–7745.
[7] H.-S. Choi, M. P. Suh, *Angew. Chem.* **2009**, *121*, 6997–7001; *Angew. Chem. Int. Ed.* **2009**, *48*, 6865–6869.
[8] J. Rabone, Y. F. Yue, S. Y. Chong, K. C. Stylianou, J. Bacsa, D. Bradshaw, G. R. Darling, N. G. Berry, Y. Z. Khimyak, A. Y. Ganin, P. Wiper, J. B. Claridge, M. J. Rosseinsky, *Science* **2010**, *329*, 1053–1057.
[9] T. M. McDonald, D. M. D'Alessandro, R. Krishna, J. R. Long, *Chem. Sci.* **2011**, *2*, 2022–2028.
[10] S. R. Caskey, A. G. Wong-Foy, A. J. Matzger, *J. Am. Chem. Soc.* **2008**, *130*, 10870–10871.
[11] S. Henke, R. A. Fischer, *J. Am. Chem. Soc.* **2011**, *133*, 2064–2067.
[12] M. Higuchi, D. Tanaka, S. Horike, H. Sakamoto, K. Nakamura, Y. Takashima, Y. Hijikata, N. Yanai, J. Kim, K. Kato, Y. Kubota, M. Takata, S. Kitagawa, *J. Am. Chem. Soc.* **2009**, *131*, 10336–10337.
[13] L.-H. Xie, M. P. Suh, *Chem. Eur. J.* **2011**, *17*, 13653–13656.
[14] H. J. Park, Y. E. Cheon, M. P. Suh, *Chem. Eur. J.* **2010**, *16*, 11662–11669.
[15] X. Kong, E. Scott, W. Ding, J. A. Mason, J. R. Long, J. A. Reimer, *J. Am. Chem. Soc.* **2012**, *134*, 14341–14344.
[16] T. M. McDonald, W. R. Lee, J. A. Mason, B. M. Wiers, C. S. Hong, J. R. Long, *J. Am. Chem. Soc.* **2012**, *134*, 7056–7065.
[17] D. H. Hong, M. P. Suh, *Chem. Commun.* **2012**, *48*, 9168–9170.
[18] H. J. Park, M. P. Suh, *Chem. Sci.* **2013**, *4*, 685–690.
[19] H. J. Park, M. P. Suh, *Chem. Commun.* **2012**, *48*, 3400–3402.
[20] J. J. Ravichandar Babarao, *J. Am. Chem. Soc.* **2009**, *131*, 11417–11425.
[21] H. J. Park, D.-W. Lim, W. S. Yang, T.-R. Oh, M. P. Suh, *Chem. Eur. J.* **2011**, *17*, 7251–7260.
[22] E. Y. Lee, S. Y. Jang, M. P. Suh, *J. Am. Chem. Soc.* **2005**, *127*, 6374–6381.
[23] H. K. Chae, J. Kim, O. D. Friedrichs, M. O'Keefe, O. M. Yaghi, *Angew. Chem.* **2003**, *115*, 4037–4039; *Angew. Chem. Int. Ed.* **2003**, *42*, 3907–3909.
[24] A. L. Spek, PLATON99, Utrecht University, Utrecht (The Netherlands), **1999**.
[25] F. Rouquerol, J. Rouquerol, K. Sing, *Adsorption by Powders, Porous Solids Principles, Methodology and Applications*, Academic Press, San Diego, CA, **1999**.
[26] G. Horváth, K. Kawazoe, *J. Chem. Eng. Jpn.* **1983**, *16*, 470–475.
[27] L. Czepirski, J. Jagiello, *Chem. Eng. Sci.* **1989**, *44*, 797–801.
[28] E. Haldoupis, S. Nair, D. S. Sholl, *J. Am. Chem. Soc.* **2012**, *134*, 4313–4323.
[29] S. Yang, X. Lin, A. J. Blake, K. M. Thomas, P. Hubberstey, N. R. Champness, M. Schröder, *Chem. Commun.* **2008**, 6108–6110.
[30] "Zeolitelike Metal–Organic Frameworks (ZMOFs): Design, Structure, and Properties": M. H. Alkordi, M. Eddaoudi, in *Supramolecular Chemistry: From Molecules to Nanomaterials*, Wiley, **2012**.
[31] A. Demessence, D. M. D'Alessandro, M. L. Foo, J. R. Long, *J. Am. Chem. Soc.* **2009**, *131*, 8784–8786.
[32] S. D. Burd, S. Ma, J. A. Perman, B. J. Sikora, R. Q. Snurr, P. K. Thallapally, J. Tian, L. Wojtas, M. J. Zaworotko, *J. Am. Chem. Soc.* **2012**, *134*, 3663–3666.
[33] N. C. Burtch, H. Jasuja, D. Dubbeldam, K. S. Walton, *J. Am. Chem. Soc.* **2013**, *135*, 7172–7180.
[34] G. Bordeau, R. Lartia, G. Metge, C. Fiorini-Debuisschert, F. Charra, M.-P. Teulate-Fichou, *J. Am. Chem. Soc.* **2008**, *130*, 16836–16837.
[35] A. J. Arvai, C. Nielsen, ADSC Quantum-210 *ADX Program*, Area Detector System Corporation; Poway, CA, USA, **1983**.
[36] Z. Otwinowski, W. Minor, in *Methods in Enzymology, Vol. 276, Part A* (Eds.: C. W. Carter, Jr., R. M. Sweet, Academic Press, New York, **1997**, p. 307.
[37] G. M. Sheldrick, *Acta Crystallogr. Sect A* **2008**, *64*, 112–122.
[38] G. M. Sheldrick, SHELEX97, Program for the crystal structure refinement, University of Göttingen: Göttingen (Germany), **1997**.
[39] G. M. Sheldrick, *Acta Crystallogr. A* **1990**, *46*, 467–473.
[40] The software package is available online at http://www.r-project.org.
[41] A. L. Myers, J. M. Prausnitz, *AIChE J.* **1965**, *11*, 121_127.

Received: August 5, 2013
Published online: November 8, 2013

